Fermi surface of ReO_3 above the "compressibility-collapse" transition

J. E. Schirber
Sandia National Laboratories, Albuquerque, New Mexico 87185

L. F. Mattheiss
Bell Laboratories, Murray Hill, New Jersey 07974
(Received 2 March 1981)

The ReO_3 Fermi surface above the pressure-induced "compressibility-collapse" transition is derived from the simple cubic band structure, assuming $T_h^5(Im3)$ symmetry for the distorted phase. A new set of closely spaced de Haas–van Alphen (dHvA) frequencies have been observed which are consistent with this model. Magnetic-breakdown effects dominate the dHvA data at higher magnetic fields. As a result, only three relatively low frequencies, all involving orbits on the new first-zone hole surface, have been detected thus far.

I. INTRODUCTION

Recently, a novel second-order phase change has been identified[1] in ReO_3 in which the compressibility increases discontinuously by a factor of about 7 upon entering the high-pressure phase. This transition was first detected by Razavi *et al.*[2] in pressure studies of the Fermi surface. These results indicated a sharp increase in the pressure derivatives of several cross-sectional areas of the Fermi surface near 3 kbar. Anomalous behavior indicative of an incipient phase transition or lattice instability had been reported previously in elastic-constant[3] and thermal-expansion[4] data as a function of temperature.

The study by Schirber and Morosin[1] included extremely accurate measurements of the pressure derivatives of the strongest de Haas–van Alphen (dHvA) frequency (corresponding to extremal orbits on the α Fermi-surface sheet in Fig. 1) which showed a very sharp break at a pressure of 2.45 kbar and displayed no hysteresis. They also reported a measurement of the room-temperature lattice constant at pressures up to ~ 80 kbar which indicated a large increase in compressibility in the 15–80-kbar range compared to the value determined previously at pressures less than 4–5 kbar.

Schirber, Azevedo, and Narath[5] subsequently used first- and second-order quadrupolar effects on the Re NMR to show that the symmetry at the Re site above the transition was lower than cubic. The first-order effect was utilized to map out the phase-transition boundary from the 2.45-kbar value at He temperatures up to a value of 5.5 kbar at 300 K. These data impose several restrictions on the space group for the distorted structure: (i) the unit cell contains only a single Re site; (ii) the point symmetry at this Re site is noncubic; and (iii) the unit cell retains overall cubic symmetry.

The simplest structure that accomodates all of these requirements has the symmetry of the $T_h^5(Im3)$ space group with a body-centered (bcc) Bravais lattice and a doubled lattice parameter. This distorted structure allows a displacement of the O atoms and produces a buckling of the previously linear Re–O –Re bond directions. It is attractive in that such buckling effects can readily explain the unexpected increase in compressibility. This structure is consistent with the $a^+a^+a^+$ distortion discussed by Clarke[6] for the sodium tungsten bronzes which involves rotation of the O octahedra about the coordiate axes.

At this point, a remaining puzzle was the fact that the ReO_3 Fermi surface appeared to be identical both above and below the transition, despite the existing evidence for a phase change. The observed dHvA frequencies at all pressures corresponded to orbits on the simple-cubic Fermi surface, with only the derivative of their variation with pressure changing. This dilemma was removed by Schirber and Overmyer[7] with the observation of the magnetic breakdown at very low fields of the dHvA signal for

a very small orbit on the distorted ReO_3 Fermi surface. It was found that these dHvA oscillations disappeared as the magnetic field was increased, presumably because magnetic breakdown[8] allowed the electrons to tunnel through the small superlattice gaps. The magnetic fields required to observe the larger extremal orbits on the distorted Fermi surface appear to be well above this breakdown field so that only the simple-cubic Fermi surface is observed and the structural change has no apparent effect.

In this paper we discuss the ReO_3 band structure and Fermi surface in the proposed high-pressure phase and present new dHvA data for a second set of orbits on the distorted Fermi surface which produce a pair of closely spaced dHvA frequencies. In Sec. II we review the ReO_3 band structure and Fermi surface in the original cubic structure and map out the new Fermi surface that is appropriate for the T_h^5 phase. Sec. III contains a description of our experimental technique as well as a presentation, discussion, and interpretation of the pair of new dHvA frequencies.

II. SUPERLATTICE EFFECTS

In this section, we analyze the effects of the T_h^5 superlattice on the simple-cubic ReO_3 Fermi surface. This O_h^1 to T_h^5 phase transition causes a doubling of the cubic lattice parameter and changes the Bravais lattice of the primitive cell from simple cubic (sc) to body-centered cubic (bcc). The number of ReO_3 molecules per primitive cell increases from one to four. Since each ReO_3 molecule contributes one conduction electron, the T_h^5 phase has four conduction electrons per primitive cell compared to one in the O_h^1 phase.

In this distorted T_h^5 phase, the Re atoms remain at their cubic positions while the O atoms are displaced in planes perpendicular to the nearest-neighbor $\langle 100 \rangle$ Re—Re bond directions. As a result, the linear Re—O—Re bonds of the cubic O_h^1 phase are buckled in the distorted T_h^5 phase and the point-group symmetry at the Re and O sites is reduced from O_h to C_{3i} and D_{4h} to C_s, respectively.

This buckling provides an attractive explanation for the "compressibility-collapse" transition in ReO_3. Namely, it suggests that the observed volume changes are the result primarily of increased buckling angles and involve only minor variations in the nearest-neighbor Re—O bond distance.

We can obtain a rough estimate of the extent of this buckling by using the measured[1] high-pressure value of the compressibility $K \approx 30 \times 10^{-4}$ kbar^{-1} and assuming that the Re—O bond distance is unchanged above the transition. At a pressure of 5 kbar (or 2.5 kbar above the transition at 1 K), the Re—O bond-buckling angle (relative to $\langle 100 \rangle$) is calculated to be about 4°.

In general, one expects such variations in bond angle to have a smaller effect on the band structure than comparable changes in the nearest-neighbor bond distances. This suggests that superlattice effects for this type of distortion may be relatively small and a useful starting point for interpreting the ReO_3 Fermi surface in the distorted phase can be derived from the simple-cubic energy-band and Fermi-surface results.

The calculated[9] Fermi surface for sc ReO_3 is shown in Fig. 1. It consists of three separate electronlike sheets which are centered at the Brillouin-zone center Γ. These are labeled α, β, and γ, respectively. The α and β sheets are closed and roughly spherical while γ is multiply connected with a "jungle-gym" topology. The intersection of these Fermi-surface sheets with the $\{100\}$ and $\{110\}$ symmetry planes of the Brillouin zone (BZ) is shown in Fig. 2. The observed cross sections and effective-mass ratios from several sources in the literature are compiled in Table I for comparison purposes.

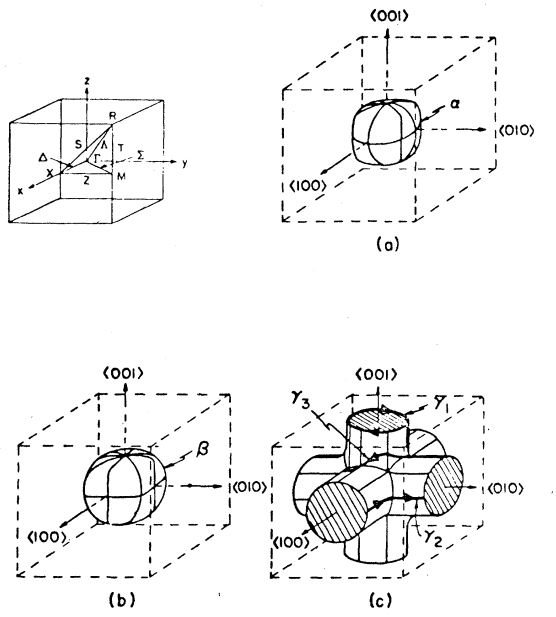

FIG. 1. Three-dimensional sketch of the normal-volume simple-cubic Fermi surface of ReO_3.

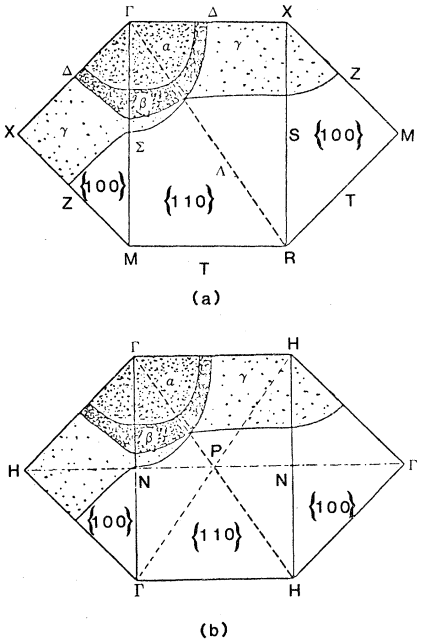

FIG. 2. (a) Central {110} and {100} cross sections of the simple-cubic ReO_3 Fermi surface, (b) simple-cubic ReO_3 Fermi surface indicating superlattice boundaries (broken lines) and bcc notation.

In the distorted T_h^5 phase, the Bravais lattice is changed to bcc and the corresponding BZ is shown to the upper left in Fig. 3. The energy bands $E(k)$ and the Fermi surface no longer have full cubic symmetry. Symmetry-related sectors of the BZ are indicated by cross hatched and unshaded surface areas.

In the limit of zero buckling angle, the primitive T_h^5 unit cell is identical with a nonprimitive cell for the O_h^1 structure. The band structure and Fermi surface for the former can be obtained by an appropriate folding of the sc results into the bcc BZ. As shown in Fig. 2(b), this involves folding the three M points of the sc BZ into Γ, the center of the bcc BZ.

The topology of the resulting Fermi surface is shown in Fig. 3. This remapped Fermi surface again occupies three zones. It consists of holes in the first and second zones (labeled h_1 and h_2, respectively) and electrons in the third zone (e_3). The contours in Fig. 3 depict the intersection of these sheets with the symmetry planes of the bcc BZ.

The shape of the second- and third-zone Fermi-surface sheets are rather similar. Each consists of closed electron surfaces centered at the Γ and H points. The topology of the first-zone hole surface h_1 is more complicated. A three-dimensional sketch of this surface is contained in Fig. 4. It consists of an array of "jack-shaped" objects centered at P which are interconnected by narrow arms along $\langle 100 \rangle$ directions.

The two smallest extremal orbits on this remapped Fermi surface occur on the h_1 sheet and are shown in Fig. 4. The first, labeled $\overline{\gamma}_2$, is a tiny neck orbit centered at N which has an area $S \approx 0.002$ Å^{-2} when $\vec{H} \parallel \langle 100 \rangle$. This magnitude is fortuitously close to the observed value.[7] The second, labled $\overline{\gamma}_4$, is an extremal orbit centered at P when $\vec{H} \parallel \langle 111 \rangle$. It is oriented so that three $\langle 100 \rangle$ arms extend above and below the orbit plane and its

TABLE I. Fermi-surface data for normal-volume ReO_3. Frequencies are from Ref. 12 and masses from Ref. 14, unless otherwise noted.

Orbit	Field direction	Frequency (in 10^6 G)	Effective-mass ratio
α	[001]	41.5	0.57
	[111]	46.3	0.69
	[110]	46.3	0.69
γ_1	[001]	48.8	0.62
	[110]	71.1	0.93
β	[001]	61.6	0.78
	[111]	73.2	
	[110]	70.3	0.89
γ_2	[001]	87.8	
γ_3	[111]	133.3	1.8[a]
γ_4	[111]	255.5	

[a]This work.

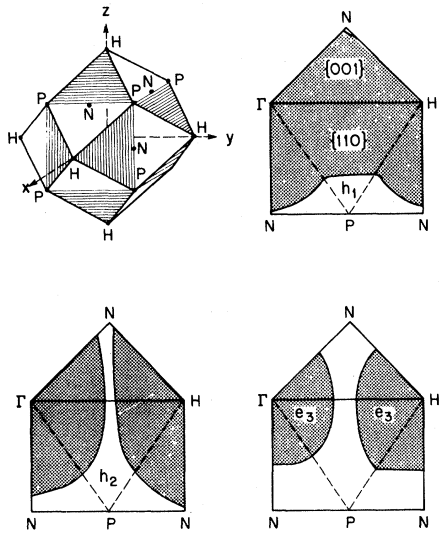

FIG. 3. Central {110} and {100} cross sections of the proposed high-pressure-phase Fermi surface of ReO_3.

area $S \approx 0.15$ Å^{-2} in a plane through the point P. Depending on the detailed shape of h_1, this central $\overline{\gamma}_4$ orbit could represent either a minimum or maximum area. The latter possibility would allow slightly smaller extremal orbits in parallel {111} planes above and below the central one and is consistent with the dHvA data that is presented in the following section.

III. EXPERIMENTAL RESULTS AND DISCUSSION

The sample used in this work (a $0.5 \times 0.5 \times 2.0$ mm^3 parallelepiped) is the same as that used earlier[1] and was obtained by iodine-vapor transport. The crossed-coil pressure-vessel geometry described in Ref. 1 was again used in this study. Pressure to 10 kbar was generated[10] in solid He and the Fermi-surface cross sections were determined from de Haas–van Alphen data using standard field-modulation techniques[11] in a 100-kOe split superconducting solenoid.

As described in Sec. II, the h_1 sheet of the distorted ReO_3 Fermi surface gives rise to the previously reported[7] $\overline{\gamma}_2$ neck oscillations. In addition, the topology of h_1 also supports a larger orbit centered on the point P when $\vec{H} \parallel \langle 111 \rangle$. In the case of the cubic Fermi surface, the similar topology of six intersecting $\langle 100 \rangle$-directed hole arms produces the γ_4 oscillations reported by Phillips and Shanks.[12] Rough scaling of the analogous dimensions of h_1 indicates that the corresponding frequencies in the distorted phase would be about $\gamma_4/16$ or ~ 16 MG.

Careful searching at fields below 60 kG with the modulation adjusted to null out the extremely strong α frequency disclosed a pair of frequencies at 13.6 and 14.5 MG. Above 50 kG, despite our best efforts, the signal was swamped by the α frequency. We could follow these low frequencies, which we label $\overline{\gamma}'_4$, and $\overline{\gamma}_4$, down to about 15 kG before they washed out.

In Fig. 5, we plot the amplitude of these $\overline{\gamma}_4$ oscillations versus reciprocal field. Ideally, this should be a straight line whose *negative* slope is proportional to the scattering or Dingle temperature. Instead the amplitude *decreases* with increasing field over the entire range of observation. The source of this unusual behavior is shown much more clearly in the

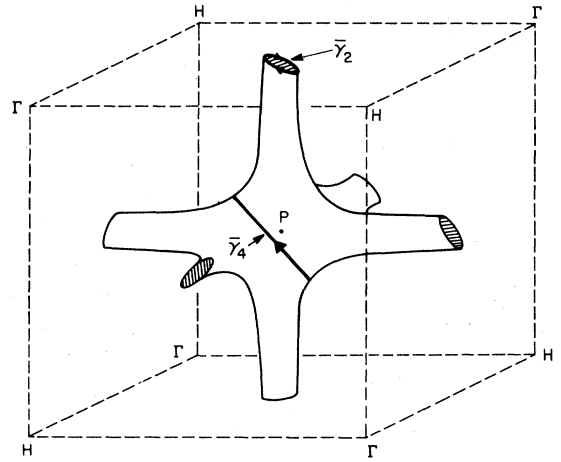

FIG. 4. Three-dimensional sketch of the h_1 sheet of the high-pressure-phase ReO_3 Fermi surface.

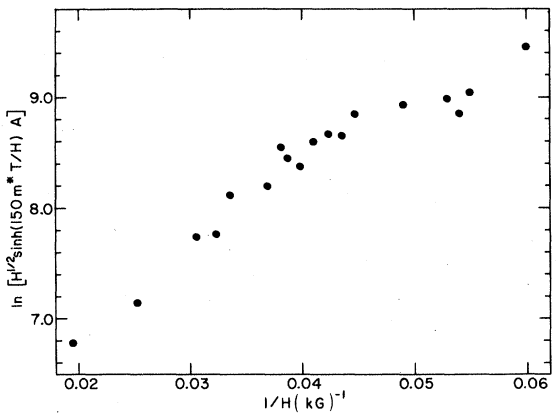

FIG. 5. Dingle plot for the $\overline{\gamma}_4$ frequency of ReO_3 at ~ 8.5 kbar for $\vec{H} \parallel$ [111] and $T \sim 1.1$ K.

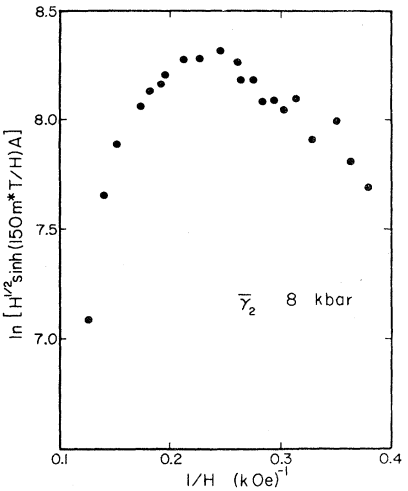

FIG. 6. Dingle plot for the $\overline{\gamma}_2$ frequency of ReO_3 at ~ 8 kbar for $\vec{H} \parallel$ [100] and $T \sim 1.1$ K.

corresponding data for $\overline{\gamma}_2$ in Fig. 6. Here, the plot exhibits a well-defined maximum in amplitude which is characteristic of magnetic breakdown. In the case of the $\overline{\gamma}_4$ data, the oscillations are just too weak to observe at fields at and below the breakdown field. The temperature dependence of the amplitude yields an effective mass of 0.55 for the $\overline{\gamma}_4$ frequencies.

The angular dependence of the $\overline{\gamma}_2$ oscillations was found[7] to vary roughly as sec θ, as expected from Fig. 4. The angular dependence of the $\overline{\gamma}_4$ oscillations is not easily determined because it actually consists of two frequencies which are beating every 16 cycles. As noted in Sec. II, these probably correspond to central ($\overline{\gamma}_4$) and noncentral ($\overline{\gamma}'_4$) orbits on the h_1 sheet centered at P. Our data for the high-pressure phase are summarized in Table II.

The amplitude of the dHvA signals is given by

$$A = H^{-1/2}(1 - e^{-H_0/H})^{n/2}(\sinh 150m^*T/H)^{-1} \times \exp(-150m^*X_D/H) \quad (1)$$

according to the standard Lifshitz-Kosevich[13] treatment. Here H is the magnetic field, m^* is the effective-mass ratio, T is the temperature, X_D is the Dingle temperature, and n is the number of tunnel

TABLE II. Fermi-surface data for high-pressure phase of ReO_3 .

Orbit	Field direction	Frequency (in 10^6 G)	Effective-mass ratio
$\overline{\gamma}_2$	[001]	0.26	0.083
$\overline{\gamma}_4$	[111]	13.6	0.55
$\overline{\gamma}_4$	[111]	14.5	

junctions in the breakdown orbit. The maximum in the plot of $\ln[H^{1/2}\sinh(150m^*T/H)A]$ vs $1/H$ is given by

$$e^{H_0/H_m} = 1 + nH_0/(300m^*X_D) \ ,$$

where H_m is the field at the maximum. As we have discussed previously,[7] it is virtually impossible to uniquely determine H_0 and X_D under these conditions because their functional dependences are so similar. Nonetheless, it is obvious that the breakdown field is extremely low, probably less than 10 kG even at our highest pressures. The breakdown field appears to decrease to even lower values as the pressure is lowered closer to the transition pressure of 2.45 kbar. This is consistent with the idea that the superlattice gaps introduced by the structural change from simple cubic to bcc increase as the Re—O—Re buckling angle increases.

The only indication at high pressure that the Fermi surface has been modified is the appearance of long-term beats in the γ_1 oscillations for $\vec{H} \parallel$ [001]. These beats occur about every 340 cycles and disappear when the pressure is lowered below the transition pressure. We do not have an explanation for this behavior.

ACKNOWLEDGMENTS

We thank D. L. Overmyer for excellent technical assistance and A. C. Switendick and W. A. Harrison for useful discussions. This work was partially supported by the U. S. Department of Energy, DOE, under Contract No. DE-AC04-76-DP00789. Sandia Laboratories is a U. S. DOE facility.

[1]J. E. Schirber and B. Morosin, Phys. Rev. Lett. 42, 1485 (1979).
[2]F. S. Razavi, Z. Altounian, and W. R. Datars, Solid State Commun. 28, 217 (1978).
[3]T. P. Pearsall and L. A. Coldren, Solid State Commun. 18, 1093 (1976).
[4]N. Matsuna, N. Yoshimi, S. Oktake, T. Akahane, and N. Tsuda, J. Phys. Soc. Jpn. 45, 1542 (1978).
[5]J. E. Schirber, L. J. Azevedo, and A. Narath, Phys. Rev. B 20, 4746 (1979).
[6]R. Clarke, Phys. Rev. Lett. 39, 1550 (1977).
[7]J. E. Schirber and D. L. Overmyer, Solid State Commun. 35, 389 (1980).
[8]A. B. Pippard, Philos. Trans. R. Soc. London Ser. A 256, 317 (1964).
[9]L. F. Mattheiss, Phys. Rev. 181, 987 (1969).
[10]J. E. Schirber, Cryogenics 10, 418 (1970).
[11]R. W. Stark and L. Windmiller, Cryogenics 8, 273 (1968).
[12]R. A. Phillips and H. R. Shanks, Phys. Rev. B 4, 4601 (1971).
[13]I. M. Lifshitz and A. M. Kosevich, Zh. Eksp. Teor. Fiz. 29, 730 (1955) [Sov. Phys.—JETP 2, 636 (1956)].
[14]F. S. Razavi and W. R. Datars, Can. J. Phys. 54, 845 (1976).